Am J Transl Res 2021;13(2):532-548
www.ajtr.org /ISSN:1943-8141/AJTR0113797

Original Article

The role of an immune signature for prognosis and immunotherapy response in endometrial cancer

Yue Meng[1], Yuebo Yang[1], Yu Zhang[1], Xiaohui Yang[1], Xiaomao Li[1], Chuan Hu[2]

[1]Department of Gynecology, The Third Affiliated Hospital of Sun Yat-sen University, Guangzhou 510000, Guangdong, China; [2]Department of Orthopaedics Surgery, The Affiliated Hospital of Qingdao University, Qingdao 266071, Shandong, China

Received May 5, 2020; Accepted December 26, 2020; Epub February 15, 2021; Published February 28, 2021

Abstract: Immunotherapy is a practical and promising treatment for advanced and recurrent endometrial cancer (EC). In this study, we identified an immune-related gene (IRG) signature to predict the overall survival (OS) and response to immune checkpoints inhibitors (ICIs) in patients with EC. The RNA expression profiles of EC were obtained from The Cancer Genome Atlas database and then were filtered for IRGs based on the Immport database. Using the conjoint Cox regression model, an immune signature consisting of seven risk IRGs (CBLC, PLA2G2A, TNF, NR3C1, APOD, TNFRSF18, and LTB) was developed. The immune signature was independent of other clinical factors and was superior to the traditional staging method for OS prediction in EC. Immunohistochemistry staining from the Human Protein Atlas database and quantitative real-time PCR analysis of EC samples were also performed to validate the expression levels of risk IRGs. By further analyzing the tumor microenvironment in EC, patients in the low-risk subgroup showed a higher immune cell infiltration status, which was associated with a better prognosis. Moreover, the tumor mutational burden and immunophenoscore analysis demonstrated that the low-risk subgroup was more sensitive to ICI-based immunotherapy. These findings might shed light on the development of targeted treatment and novel biomarkers for patients with EC.

Keywords: Immune signature, prognosis, immunotherapy, The Cancer Genome Atlas, endometrial cancer

Introduction

Endometrial cancer (EC) is the fourth most commonly diagnosed malignancy worldwide, accounting for 4.8% of all cancer diagnoses and 2% of all cancer deaths [1]. The incidence and mortality of EC have been increasing recently, with the United States reporting approximately 61,880 newly diagnosed cases and 12,160 cancer-related deaths in 2019 [2]. Standard treatment, including surgery, chemotherapy, and radiotherapy, has improved the prognosis of early-stage EC with a 5-year survival rate of 95% [3]. However, there are relatively few treatment options for advanced/recurrent EC patients, and the median survival (12 to 15 months) of these patients remains dismal [4].

The tumor microenvironment (TME) has been reported to play a pivotal role in EC tumorigenesis [5]. The increasing tumor mutational burden (TMB) and the presence of tumor-infiltrating lymphocytes in the TME have been associated with the presence of neoantigens, which contribute to the immunotherapy response in patients with EC [6]. Immune checkpoint inhibitor (ICI)-based immunotherapy targeting certain immune checkpoint blockade (ICB) such as cytotoxic T lymphocyte antigen 4 (CTLA4), programmed cell death 1 (PD1), and programmed cell death-ligand 1 (PD-L1), has proven effective for different cancers [7, 8]. However, some types of relapsed EC are refractory to ICIs [9]. In recent years, new genomic databases and high-throughput sequencing technologies have allowed the massive identification of tumor biomarkers, which are emerging as a new hope for cancer therapy [10, 11]. Hence, it is imperative to develop a predictive biomarker for prediction prognosis and immunotherapy responsiveness of EC patients.

Increasing evidence has demonstrated that immune-related genes (IRGs) have a significant impact on predicting the prognosis of cancer, such as cervical cancer [12], ovarian cancer [13], and lung cancer [14]. As little is known about the role of IRGs in EC, our efforts were concentrated on developing an immune signature based on IRGs with predictive ability for EC patients. In addition, we explored the relationship of the immune signature with tumor-infiltrating immune cells, TMB, as well as the immunophenoscore (IPS) of EC, which may provide an in-depth insight into precision treatment for this malignancy.

Material and methods

Patients and data acquisition

The gene expression profiles of 566 EC samples were retrieved from TCGA database (https://tcga-data.nci.nih.gov/tcga/). The list of 2498 IRGs were identified from the ImmPort database (http://www.immport.org/) [15]. A total of 318 cancer-related transcription factors (TFs) were downloaded from the Cistrome project (http://www.cistrome.org/) [16]. Corresponding clinical information and TMB data downloaded from TCGA were also integrated into further analysis. We matched mRNA expression data with clinical information using patients' barcodes, and patients with overall survival (OS) were less than 90 days were excluded. Ultimately, we obtained 503 EC cases for survival analysis.

Differential gene expression analysis and functional annotation

The differentially expressed genes (DEGs) and differentially expressed TFs (DETFs) between tumor tissue (n = 543) and normal tissue (n = 23) were compared using the "limma" R package (http://www.bioconductor.org/packages/release/bioc/html/limma.html) with Wilcoxon signed-rank test [17]. A false-discovery rate (FDR) < 0.05 and |log2 fold change (FC)| > 2 were defined as the thresholds. The differentially expressed IRGs (DEIRGs) were generated from the intersection of the DEGs and IRGs list. We further investigated the functions of those DEIRGs based on the Gene Ontology (GO) and Kyoto Encyclopedia of Genes and Genomes (KEGG) pathway enrichment analyses using the "clusterProfiler" R package [18]. A *P*-value < 0.05 was considered statistically significant.

Establishment of the immune signature for EC

A total of 503 patients with EC were randomly stratified into the training cohort and the testing cohort at a 1:1 ratio. The training cohort was used to develop the immune signature, while the testing cohort and total cohort were used for validating the results. In the training cohort, univariate Cox regression analysis was used to identify the prognostic DEIRGs. Next, multivariate Cox regression analysis with stepwise selection was performed to construct the prognostic immune signature for evaluating the survival of patients with EC [19]. We calculated the risk score for each patient using expression counts of risk IRGs and the regression coefficients from multivariate Cox model. This risk score was calculated using the following formula: Risk score = (expression of Gene 1 × coefficient of Gene 1) + (expression of Gene 2 × coefficient of Gene 2) + ... + (expression of Gene *n* × coefficient of Gene *n*). patients were then classified into high- and low-risk subgroups based on the median value of the risk score in the training cohort. We performed survival analysis to compare the OS between high- and low-risk groups, and displayed the results using Kaplan-Meier curves. The receiver operating characteristic (ROC) curves were used to graphically verify the discrimination of the immune signature, and an area under the ROC curve (AUC) > 0.60 was regarded as acceptable for prediction [20].

Regulatory mechanisms of prognostic DEIRGs and DETFs

TFs are directly involved in the expression of relevant IRGs [21]. The Cistrome project provides the regulatory association between the TFs and transcriptome in TCGA profiles. We constructed regulatory networks of prognostic DEIRGs and DETFs for visual analysis using a standard correlation of coefficient > 0.4 and a filter threshold of P < 0.001. The regulatory networks were presented using Cytoscape software version 3.6.1.

Independent prognosis analysis and building a nomogram

To further investigate whether the immune signature could be an independent prognostic fac-

tor in EC, we performed univariate and multivariate Cox analyses using the entire cohort by integrating the immune signature and clinical factors. Based on the results, we constructed a nomogram to predict the probability of 3- and 5-year OS of patients with EC. The predictive performance of the nomogram was visualized using the ROC curves. Moreover, correlation analysis was conducted to analyze the interactions between our immune signature (the risk score and risk IRGs) and clinical factors (age, grade, stage, histological types). A *P*-value < 0.05 denoted statistical significance.

Validation of the risk IRGs

We further evaluated the expression patterns of risk IRGs at the translational and transcriptional level. The immunohistochemistry stained maps of risk IRGs in normal and EC tissues were obtained from The Human Protein Atlas (HPA) database (https://www.proteinatlas.org/), which is an open access database available to the public for the exploration of the human proteome.

Besides, we performed quantitative real-time PCR (qRT-PCR) analysis to detect the mRNA expression levels of risk IRGs using 10 pairs of matched samples from tumor tissues and adjacent normal tissues. These samples were obtained from EC patients and immediately stored in a freezer at -80°C until use. The experiment was approved by the Ethical Committee of the Third Affiliated Hospital of Sun Yat-sen University, and all participated patients are informed consent.

Total RNA was extracted using TRIzol Reagent (Invitrogen, Carlsbad, CA, USA), and the PrimeScript™ RT reagent kit (Takara Biotech, Dalian, China) was used to react RNA and synthesize single-stranded complementary DNA according to the manufacturer's instructions. Real-time quantification was further performed using Talent qPCR PreMix (SYBR-Green) (Tiangen Biotech, Beijing, China) according to the manufacturer's protocols. The sequences of the primers used are reported in Table S1. GAPDH was used as the endogenous control. We recorded the cycle threshold (Ct) of each gene and the relative gene expressions were calculated using the 2-ΔΔCt method (ΔCt = Ct target gene-Ct internal control).

Estimation of tumor-infiltrating immune cells

Immune cells are the main components of TME and correlate with prognosis. We estimated the relative abundance of 22 types of infiltrating immune cells in EC using the CIBERSORT algorithm, which is a machine learning method based on support vector regression in gene expression data of TCGA samples [22]. The Wilcoxon rank-sum test was then used to assess the differential infiltrating density between high- and low-risk subgroups.

Mutation analysis

The mutation data containing somatic variants in TCGA were stored in mutation annotation format form and analyzed using the "maftools" R package [23]. The TMB counts for each EC sample were measured as follows: (total mutation/total covered bases) × 10^6 [24]. Differences in TMB were compared between high- and low-risk subgroups, and the higher TMB counts indicated higher sensitivity to immunotherapy [25].

Immunophenoscore analysis

The Immunophenoscore (IPS) of EC patients was retrieved from the Cancer Immunome Atlas (TCIA) (https://tcia.at/home), which reflects patients' capability to respond to ICIs [26]. Immunosuppressive cells, effector cells, MHC molecules, and immunomodulators were defined as the four components of IPS. The scale of the IPS ranged from 0-10 and was determined by summing the corresponding gene expression z-scores, whereby higher scores were positively associated with increased immunogenicity.

Statistical analysis

Categorical variables were presented as frequency (n) and proportion (%); continuous variables were described as mean ± standard error (SE). The differences in variables were tested using chi-square tests, t-tests, or nonparametric tests, as appropriate. The association of variables was assessed using Spearman's correlation coefficient test. Construction and evaluation of the immune signature were analyzed using univariate and multivariate analyses, and survival differences were compared using the log-rank test. Statistical analyses were per-

Table 1. Clinical characteristics of patients with EC

Characteristics	Group	Training cohort (n = 255)	Testing cohort (n = 248)	Total cohort (N = 503)	Statistical test	*P* value
Age (years)	≤ 65	139 (54.7%)	148 (59.5%)	287 (57.1%)	χ^2 test	0.271
	> 65	116 (45.3%)	100 (40.5%)	216 (42.9%)		
Race	White	186 (73.0%)	171 (69.0%)	357 (71.1%)	Fisher's exact test	0.541
	Black	54 (21.2%)	56 (22.6%)	110 (21.9%)		
	Asian	8 (3.1%)	14 (5.6%)	22 (4.2%)		
	Other*	7 (2.7%)	7 (2.8%)	14 (2.8%)		
Grade	G1	99 (38.8%)	102 (41.1%)	201 (39.9%)	χ^2 test	0.051
	G2	75 (29.4%)	71 (28.6%)	146 (29.0%)		
	G3	81 (31.8%)	75 (30.3%)	156 (31.1%)		
stage	Early (I&-II)	188 (73.7%)	179 (72.2%)	367 (72.9%)	χ^2 test	0.554
	Advanced (III&-IV)	67 (26.3%)	69 (27.8%)	136 (27.1%)		
Histological types	Endometroid endometrial adenocarcinoma	185 (72.5%)	191 (77.0%)	376 (74.8%)	Fisher's exact test	0.562
	Mixed serous and endometroid carcinoma	11 (4.3%)	8 (3.2%)	19 (3.7%)		
	Serous endometrial adenocarcinoma	59 (23.1%)	49 (19.8%)	108 (21.5%)		
Vital status	Alive	205 (80.4%)	212 (84.5%)	417 (82.9%)	χ^2 test	0.185
	Dead	50 (19.6%)	36 (14.5%)	86 (17.1%)		
Survival time (mean ± SE, days)		1257±60.69	1186±49.45	1222±39.20	t-test	0.364

Other*: American native, Alaska native, or Pacific islander.

formed using R software (version 3.5.2.) and Graphpad Prism 7. A *P*-value of < 0.05 for the two-sided tests was regarded statistically significant.

Results

Acquisition of DEIRGs and functional annotation

A total of 503 patients with EC were identified from the TCGA database based on the inclusion criteria. Patients were then divided into the training cohort (n = 255) and testing cohort (n = 248). As listed in **Table 1**, there were no significant differences in clinical variables between the two cohorts. A total of 2354 DEGs were identified and were included in accordance with the set standards. Of these, 175 were DEIRGs, including 108 upregulated genes and 71 downregulated genes (Figure S1). Functional enrichment analysis showed that the DEIRGs were involved in immune- or inflammation-related process. The most enriched terms in the GO analysis for cellular components, biological processes, and molecular function were "external side of plasma membrane", "cell chemotaxis", and "receptor-ligand activity", respectively (**Figure 1A**). KEGG pathways analysis demonstrated that "cytokine-cytokine receptor interaction", "chemokine signaling pathway", "MAPK signaling pathway", and "PI3K-Akt signaling pathways" were enriched in DEIRGs (**Figure 1B**).

Identification of an immune signature based on DEIRGs

To construct a prognostic immune signature, we performed univariate and multivariate Cox regression analyses based on the above 175 DEIRGs in the training cohort. By screening using the univariate analysis, 18 OS-related DEIRGs were identified (Table S2). Next, we screened these 18 prognostic DEIRGs using multivariate analysis with stepwise selection. Seven risk IRGs were selected to construct the prognostic model (**Table 2**). Four of these seven IRGs were associated with poor prognosis (CBLC, PLA2G2A, TNF, NR3C1), while the three remaining genes (APOD, TNFRSF18, LTB) served as protective factors for EC patients. The individualized risk scores weighted by the relative coefficients were calculated as follows: Risk score = (expression of CBLC × 0.013611) + (expression of TNF × 0.035927) + (expression of PLA2G2A × 0.032196) + (expression of NR3C1 × 0.165537) + (expression of APOD × -0.028888) + (expression of TNFRSF18 × -0.019835) + (expression of LTB × -0.020554). Based on this model, we calculated and ranked the risk scores for each EC patient and the median value in the training cohort was defined as the cut-off point. Subsequently, the EC

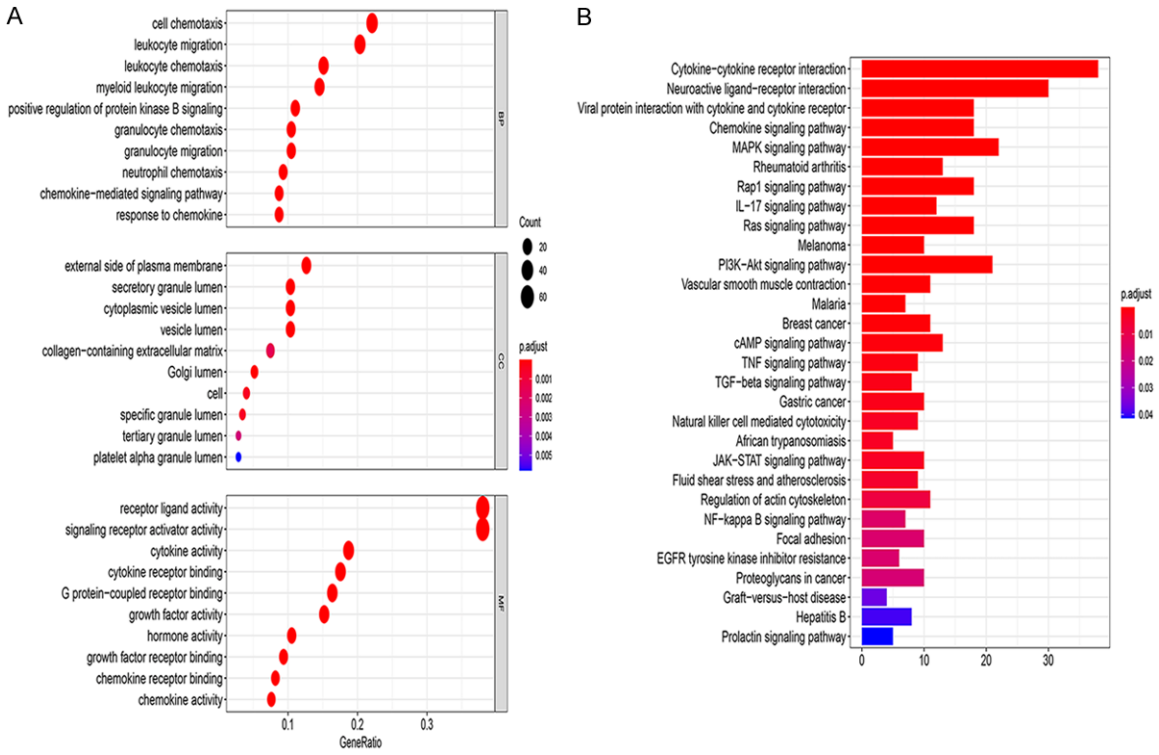

Figure 1. Functional enrichment analyses of the DEIRGs. A. The dot plot of the top 10 GO items enriched in the DEIRGs. (BP, biological process; CC, cellular component; MF, molecular function). B. The bar plot of the top 30 KEGG pathways enriched in the DEIRGs.

Table 2. Multivariate Cox regression model results of risk IRGs in immune signature

Gene	Regulation	Coefficient	HR (95% CI)	*P* value
CBLC	Up	0.013611	1.0137 (1.0065-1.0208)	0.00015
TNF	Up	0.035927	1.0365 (1.0115-1.0622)	0.00395
LTB	Up	-0.020554	0.9796 (0.9559-1.0039)	0.09986
TNFRSF18	Up	-0.019835	0.9803 (0.9511-1.0104)	0.19888
PLA2G2A	Down	0.032196	1.0327 (0.9969-1.0697)	0.07327
NR3C1	Down	0.165537	1.1801 (1.0428-1.3352)	0.00865
APOD	Down	-0.028888	0.9715 (0.9407-1.0032)	0.07822

HR: hazard ratio; CI: confidence interval.

patients in the training, testing, as well as in the overall cohort were respectively classified into high- and low-risk subgroups. The rank of the risk score, survival status, and the expression patterns of the seven risk IRGs in the EC patients of each cohort are illustrated in **Figure 2A-C**. The Kaplan-Meier survival curves showed that patients in the high-risk subgroup had worse prognosis than the low-risk subgroup ($P < 0.01$, **Figure 2D**). The ROC curves of the immune signature also showed a good predictive accuracy (**Figure 2E**). The AUCs of the immune signature in the training cohort for predicting the 1-, 3-, and 5-year survival were 0.724, 0.705, and 0.698, respectively. The results of the AUCs in the testing and total cohort were similar to those of the training cohort.

Construction of the prognostic DEIRGs-DETFs regulatory network

As mentioned above, the 18 OS-related prognostic DEIRGs were identified by conducting a univariate Cox regression analysis based on 175 DEIRGs. To further investigate the dysregulation mechanisms of EC patients, we constructed the prognostic DEIRG-DETF regulatory networks (Table S3). The resulting networks showed that 13 prognostic DEIRGs were associated with 29 DETFs in EC based on the correlation coefficient > 0.4 and $P < 0.001$ (Figure S2).

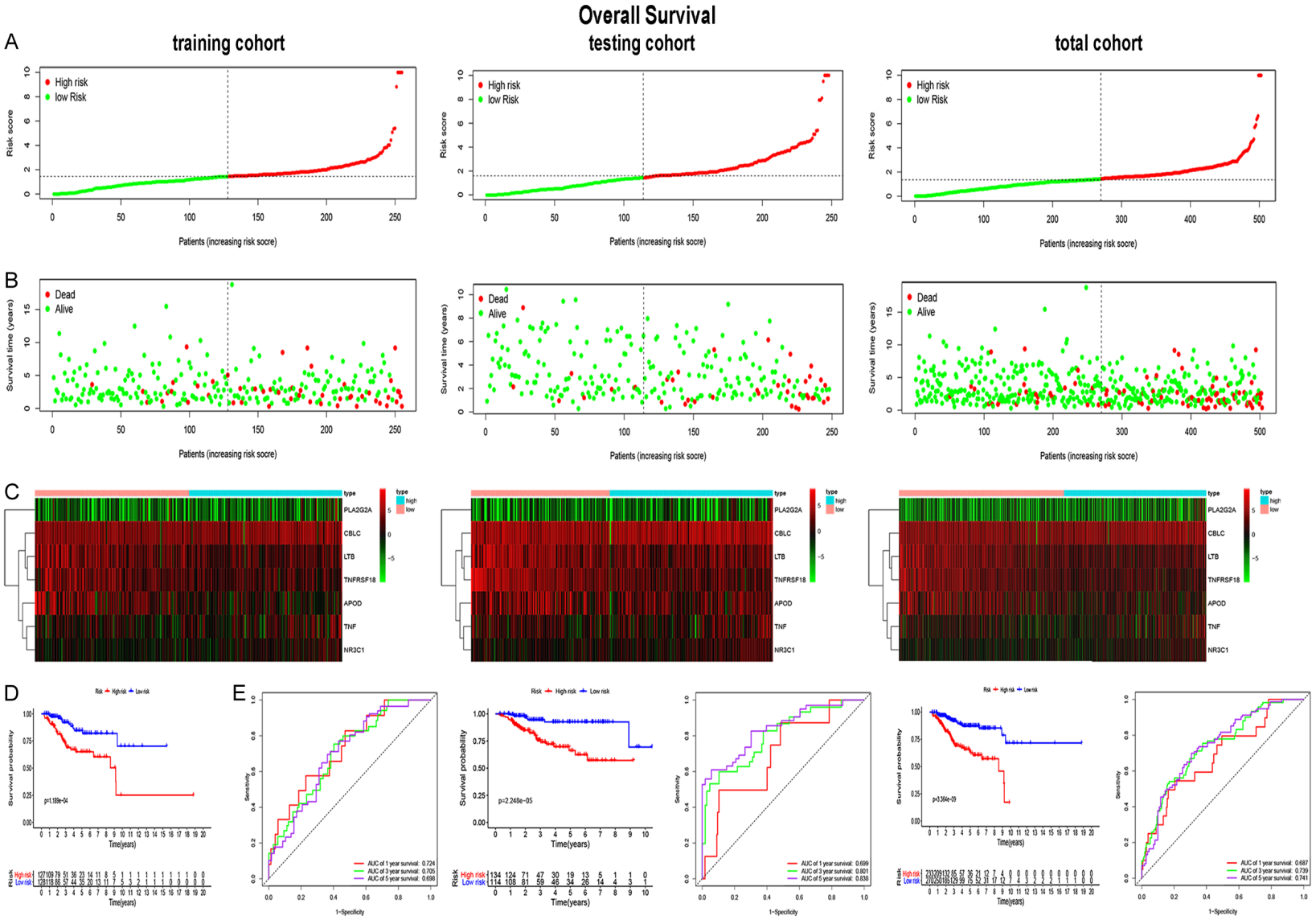

Figure 2. Identification of the prognostic immune signature in the training, testing, and total TCGA cohort. A. Distribution of the risk score in patients with EC. Patients were divided into high- and low-risk subgroups based on the median value of the calculated risk score (vertical black line). B. Scatter plots of survival status in patients with EC. C. Heatmap of risk IRG expression patterns of high- and low-risk subgroups. D. Survival analysis of the immune signature for patients with EC. E. Time-dependent ROC analysis of immune signature for patients with EC.

Table 3. Univariate and multivariate Cox regression analyses for OS in the total EC cohort

Variables	Univariate analysis		Multivariate analysis	
	HR (95% CI)	*P* value	HR (95% CI)	*P* value
Age	1.034 (1.014-1.055)	0.0006	1.025 (1.003-1.047)	0.0204
Race	0.854 (0.641-1.138)	0.2831		
Grade	2.773 (1.806-4.257)	< 0.0001	2.102 (1.334-3.310)	0.0013
Stage	3.891 (2.550-5.938)	< 0.0001	3.162 (2.013-4.968)	< 0.0001
Histological types	1.720 (1.385-2.135)	< 0.0001	1.082 (0.847-1.383)	0.524
Risk score	1.045 (1.030-1.061)	< 0.0001	1.032 (1.016-1.048)	< 0.0001

HR: hazard ratio; CI: confidence interval.

Assessment of independent prognostic and construction of the nomogram

We conducted both univariate and multivariate Cox regression analyses using the entire cohort and including clinical factors and risk score (**Table 3**). The results showed that age, stage, grade, pathological type, and risk score were independently associated with the OS in univariate analysis (P < 0.05). After adjusting for confounding factors, the multivariate analysis demonstrated that the risk score could be an independent prognostic predictor of OS in EC patients (P < 0.05). We constructed a time-dependent ROC to compare the predictive capability of the risk score and other clinical factors. The results showed that our immune signature was more accurate in predicting OS than stage, grade, or age (Figure S3). To facilitate the clinical utility of the immune signature, we built a predictive nomogram for OS with four prognostic predictors: age, stage, grade, and risk score (**Figure 3A**). Compared to the single factors alone, the integrated nomogram presented the largest AUC in the ROC analysis. The AUCs of the nomogram at 3- and 5-years were 0.785 and 0.793, respectively (**Figure 3B**, **3C**).

We also performed a correlation analysis comparing the immune signature and the clinical factors of EC in the total cohort (Table S4). The expression of NR3C1 and TNF were higher in older patients, while the expression of APOD was higher in younger patients (≤ 65 vs. > 65, P < 0.05, **Figure 4A-C**). The tumor grade increased as the levels of NR3C1, PLA2G2A, and the risk score increased, while the grade decreased as the levels of APOD, LTB, and TNFRSF8 increased (G1 vs. G2 vs. G3, all P < 0.05, **Figure 4D-I**). The expression of APOD was higher in patients with early stage disease than in those with advanced-stage, but the expression pattern of NR3C1 showed the opposite relationship (early-stage vs. advanced-stage, all P < 0.05, **Figure 4J**, **4K**). With regard to pathological types (endometrioid adenocarcinoma vs. mixed serous and endometrioid carcinoma vs. serous endometrial adenocarcinoma), the risk score was higher in mixed or serous adenocarcinoma, while the expression of NR3C1 and TNF were significantly higher in mixed and serous endometrial carcinoma, respectively, whereas the expression of APOD and TNFRSF18 were significantly higher in endometroid adenocarcinoma (all P < 0.05, **Figure 4L-P**). These results illustrated that the dysregulated expression of IRGs was correlated with the development of CC.

Validation of seven risk IRGs

We further verified the expression patterns of risk IRGs in terms of protein and mRNA levels. The immunohistochemistry staining from HPA showed that six risk IRGs (CBLC, LTB, TNFRSF18, PLA2G2A, NR3C1, APOD) were dysregulated in EC samples (**Figure 5A**). The expression levels of CBLC, LTB, and TNFRSF18 were higher in EC samples compared to normal samples, whereas the expression levels of PLA2G2A, NR3C1, APOD were lower in EC samples than those in normal samples. TNF was missing in the immunohistochemistry database of HPA. The mRNA expression of the seven risk IRGs were also validated using qRT-PCR in 10 pairs of matched samples obtained from EC patients (**Figure 5B**). The qRT-PCR results indicated that the relative mRNA expression of CBLC, TNF, LTB, and TNFRSF18 in tumor tissues was significantly higher than that in adjacent normal tissues, whereas the relative mRNA expression of PLA2G2A and APOD was significantly lower in tumor tissues compared to adjacent normal tissues (all P < 0.05).

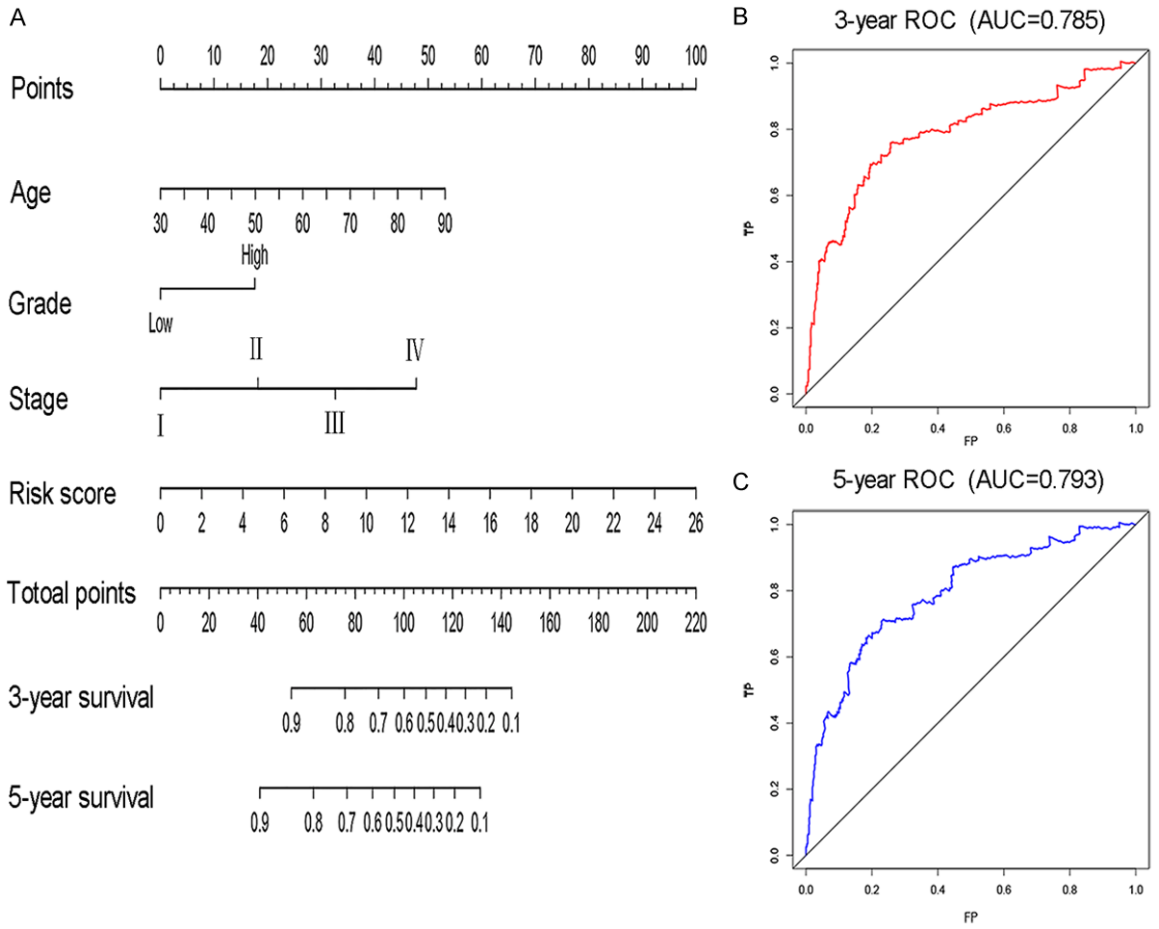

Figure 3. Nomogram and ROC curves for predicting the prognosis of EC at 3- and 5-years. A. Nomogram for predicting OS. There are four factors in this nomogram: age, grade, stage, and risk score. Each of them generates points according to the line drawn upward. And the total points of the four factors of an individual patient lie on "Total Points" axis which corresponds to the probability of OS rates at 3- and 5-years. B. ROC curves for OS at 3-years. C. ROC curves for OS at 5-years.

However, there was no significant difference in terms of NR3C1 expression ($P > 0.05$).

TME changes associated with immune signature in EC

To reveal the correlations of the TME with immune signature in EC, we analyzed differences in the presence of tumor-infiltrating immune cells in the high- and low-risk subgroups using the CIBERSORT algorithm. Among the 22 immune cell types, B cells naïve, macrophages M1, and dendritic cells activated were positively correlated with the risk score, while T cells CD8, T cells regulatory (Tregs), NK cells activated, and dendritic cells resting were negatively correlated with the risk score (**Figure 6A**). Furthermore, the higher proportion of T cells CD8, Tregs, NK cells activated, and dendritic cells resting were significantly associated with better prognosis for EC in the survival analyses (**Figure 6B**). These results may partially explain the poorer prognosis of patients in the high-risk subgroups.

The immune signature and mutation profile

The landscape of the mutation profile in EC is displayed in **Figure 7A**. The top 10 frequently mutated genes in EC patients were: PTEN, PIK3CA, ARID1A, TTN, TP53, PIK3R1, KMT2D, CTCF, MUC16, and CTNNB1. We found that TMB was higher in the low-risk subgroup than in the high-risk subgroup ($P = 0.004$, **Figure 7B**). Moreover, patients with a higher TMB had a better prognosis than those with low TMB,

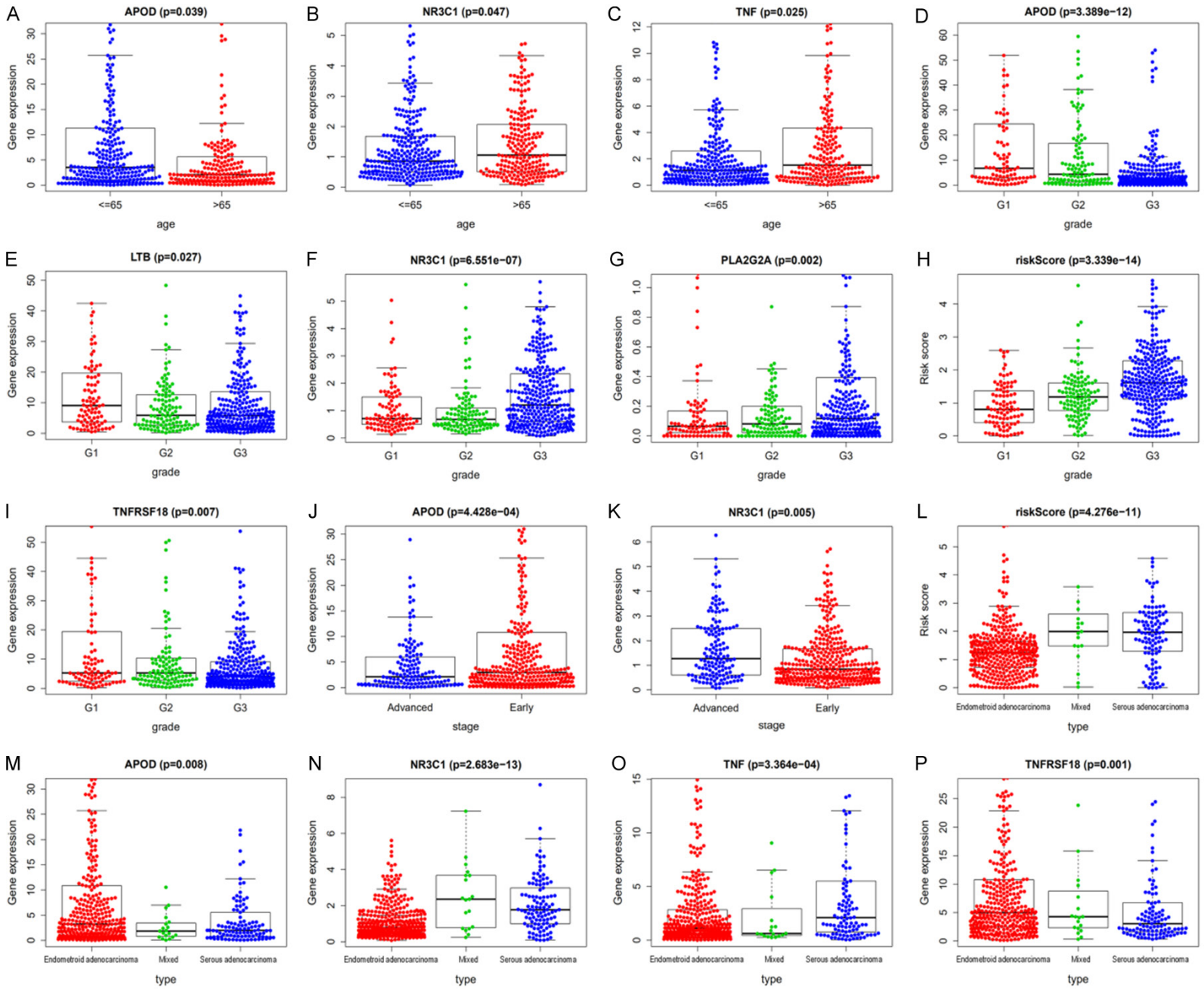
A
APOD (p=0.039)
Gene expression
<=65
>65
age
B
NR3C1 (p=0.047)
Gene expression
<=65
>65
age
C
TNF (p=0.025)
Gene expression
<=65
>65
age
D
APOD (p=3.389e−12)
Gene expression
G1
G2
G3
grade
E
LTB (p=0.027)
Gene expression
G1
G2
G3
grade
F
NR3C1 (p=6.551e−07)
Gene expression
G1
G2
G3
grade
G
PLA2G2A (p=0.002)
Gene expression
G1
G2
G3
grade
H
riskScore (p=3.339e−14)
Risk score
G1
G2
G3
grade
I
TNFRSF18 (p=0.007)
Gene expression
G1
G2
G3
grade
J
APOD (p=4.428e−04)
Gene expression
Advanced
Early
stage
K
NR3C1 (p=0.005)
Gene expression
Advanced
Early
stage
L
riskScore (p=4.276e−11)
Risk score
Endometroid adenocarcinoma
Mixed
Serous adenocarcinoma
type
M
APOD (p=0.008)
Gene expression
Endometroid adenocarcinoma
Mixed
Serous adenocarcinoma
type
N
NR3C1 (p=2.683e−13)
Gene expression
Endometroid adenocarcinoma
Mixed
Serous adenocarcinoma
type
O
TNF (p=3.364e−04)
Gene expression
Endometroid adenocarcinoma
Mixed
Serous adenocarcinoma
type
P
TNFRSF18 (p=0.001)
Gene expression
Endometroid adenocarcinoma
Mixed
Serous adenocarcinoma
type

Figure 4. The correlation between the immune signature and clinical factors of patients with EC in the TCGA cohort. A-C. Differences in expression of APOD, NR3C1, and TNF in terms of age (≤ 65 or > 65 years). D-I. Differences in the expression of APOD, LTB, NR3C1, PLA2G2A, risk score, and TNFRSF18 across pathological grades (G1, G2, and G3). J, K. Differences in expression of APOD and NR3C1 between the pathological stage (early/advanced). L-P. Differences in the expression of the risk score, APOD, NR3C1, TNF, and TNFRSF18 across histological types (endometrioid endometrial adenocarcinoma, mixed serous and endometrioid carcinoma, and serous endometrial carcinoma).

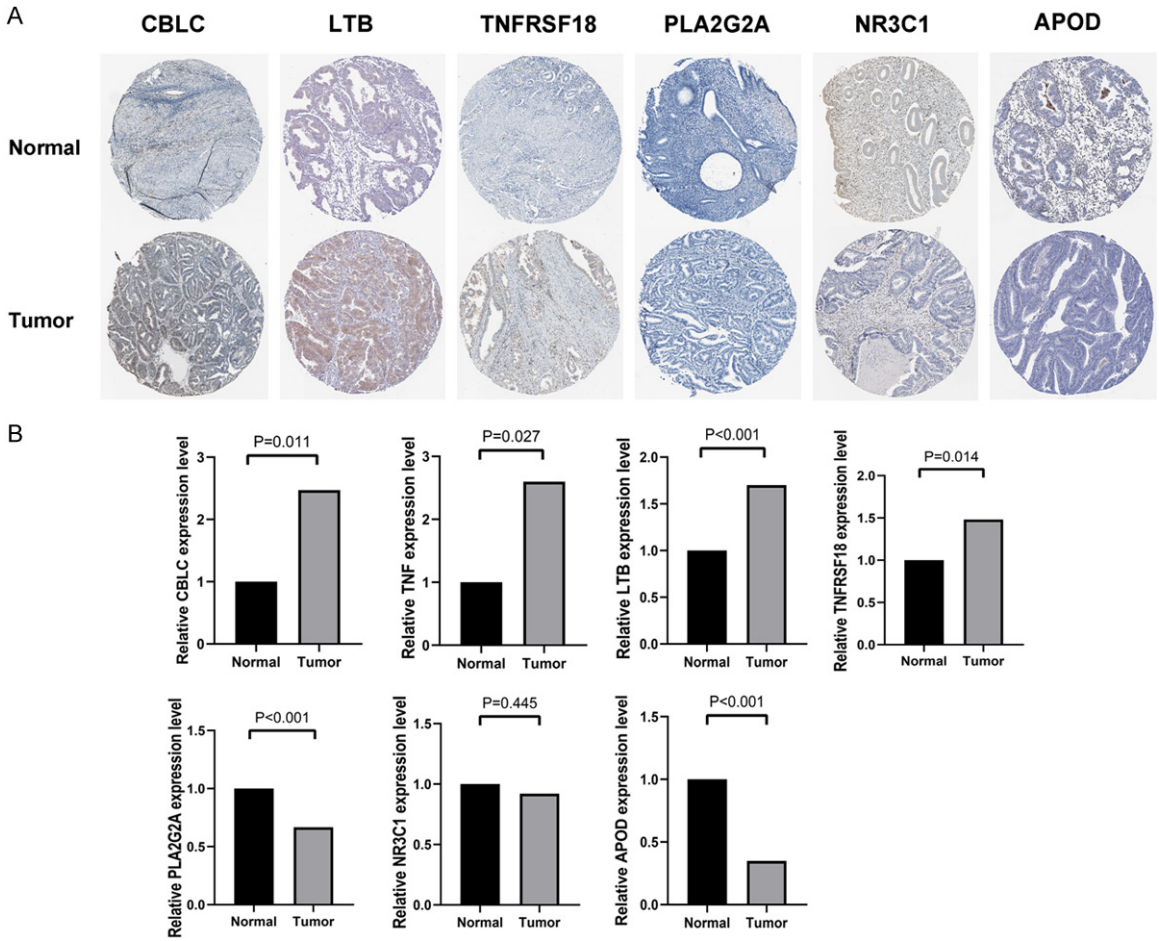

Figure 5. Validation of the risk IGRs expression at the protein and mRNA levels. A. Immunohistology assay of the risk IGRs using data from the HPA database. Protein levels of CBLC in normal tissue (staining: not detected; intensity: negative; quantity: none) and tumor tissue (staining: low; intensity: moderate; quantity: < 25%). Protein levels of LTB in normal tissue (staining: not detected; intensity: negative; quantity: none) and tumor tissue (staining: medium; intensity: moderate; quantity: > 75%). Protein levels of TNFRSF18 in normal tissue (staining: not detected; intensity: negative; quantity: none) and tumor tissue (staining: medium; intensity: moderate; quantity: 75%-25%). Protein levels of PLA2G2A in normal tissue (staining: low; intensity: moderate; quantity: < 25%) and tumor tissue (staining: not detected; intensity: negative; quantity: none). Protein levels of NR3C1 in normal tissue (staining: medium; intensity: strong; quantity: < 25%) and tumor tissue (staining: not detected; intensity: negative; quantity: none). Protein levels of APOD in normal tissue (staining: low; intensity: moderate; quantity: < 25%) and tumor tissue (staining: not detected; intensity: negative; quantity: none). B. qRT-PCR results of the expression of CBLC, TNF, LTB, TNFRSF18, PLA2G2A, NRC31, and APOD in 10 matched samples from EC tissues and adjacent normal tissues.

although this difference was not statistically significant (P = 0.138, **Figure 7C**).

Stratification of patients to immunotherapy

Previous studies have demonstrated that the IPS was correlated with responses to ICI-based immunotherapy [27]. In the present study, we comprehensively explored the correlation of our immune signature with the IPS in EC patients. Scores for IPS, IPS-CTLA4, IPS-PD1/PD-L1/PDL2 + CTLA4, and IPS-PD1/PD-L1/PD-L2 were calculated to assess the potential for beneficial treatment with ICIs in EC patients.

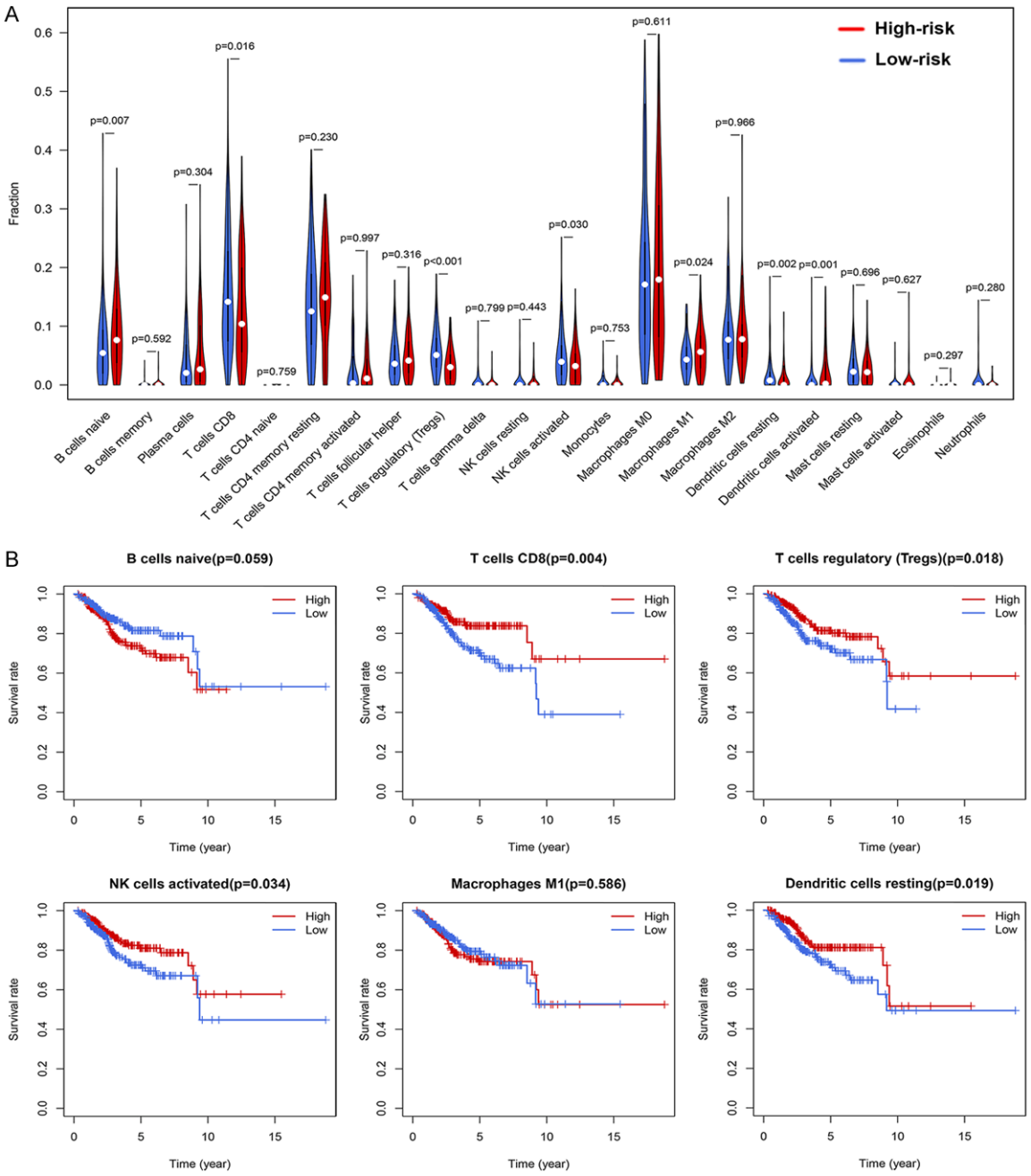

Figure 6. Association between the immune signature and tumor-infiltration of immune cells in EC based on the TCGA dataset. A. Violin plots showing the relative proportion of 22 immune cell types in high- and low-risk subgroups. The white dots inside the violin represent the median values. B. Kaplan-Meier curves showing the correlation of immune cell infiltration and OS for patients with EC, including naive B cells, CD8 T cells, Tregs, activated NK cells, M1 macrophages, and resting dendritic cells.

As shown in **Figure 8A**, patients in the low-risk subgroup had relatively higher scores in all four categories ($P < 0.0001$). Meanwhile, patients in the low-risk subgroup were associated with the higher expression of PD1 and CTLA4 ($P < 0.0001$, **Figure 8B**). The expression of PD-L2 and PD-L1 was also higher in the low-risk subgroup. However, the differences were not statistically significant. These results indicated that patients in the low-risk subgroup expressed a more immunogenic phenotype and were promising candidates for ICIs.

Discussion

Increasing evidence suggests that the TME contributes to cancer proliferation and progres-

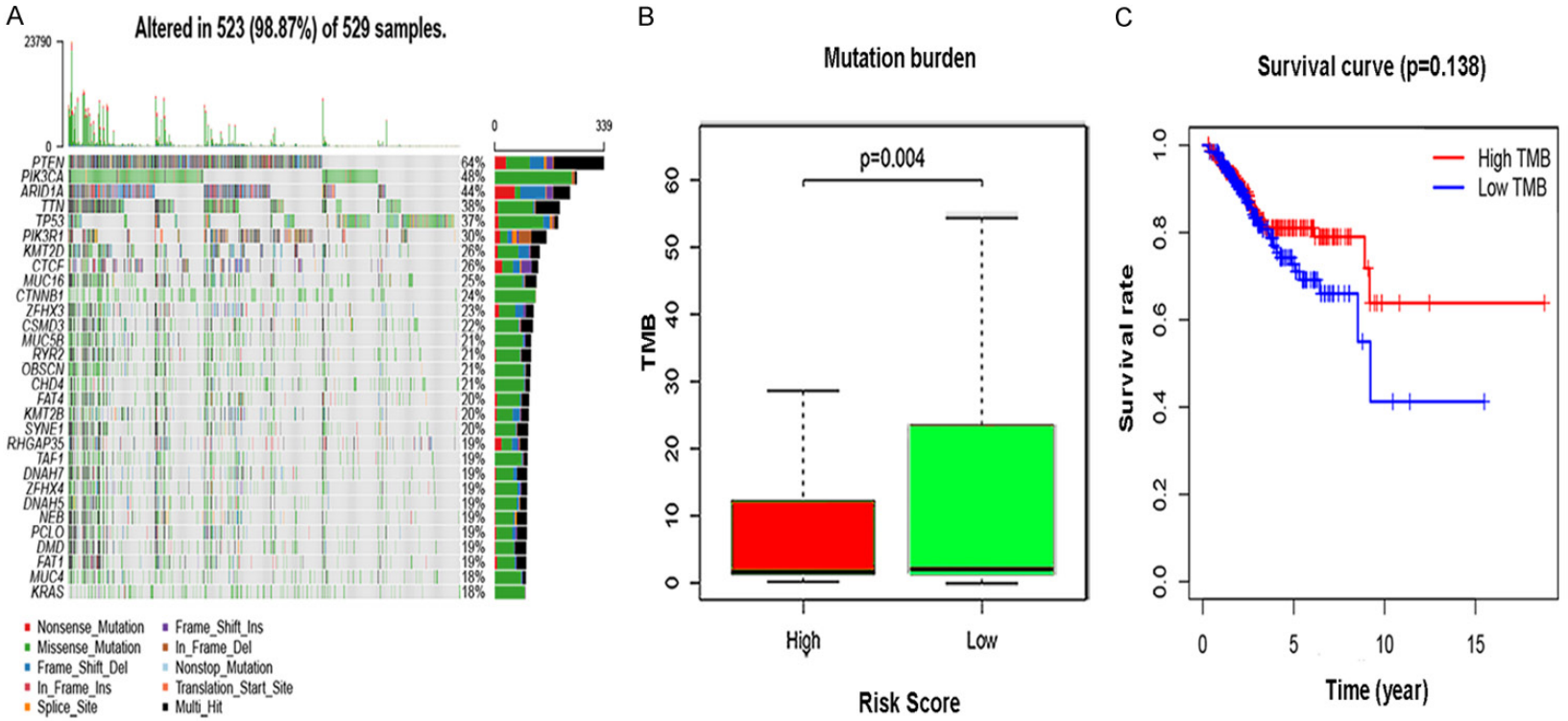

Figure 7. Mutational analysis of patients with EC. A. Waterfall plots of the mutational profile in the EC patient cohort. B. Kaplan-Meier curves showing the association of TMB and OS. C. Comparison of the TMB counts stratifying patients into high- and low-risk subgroups.

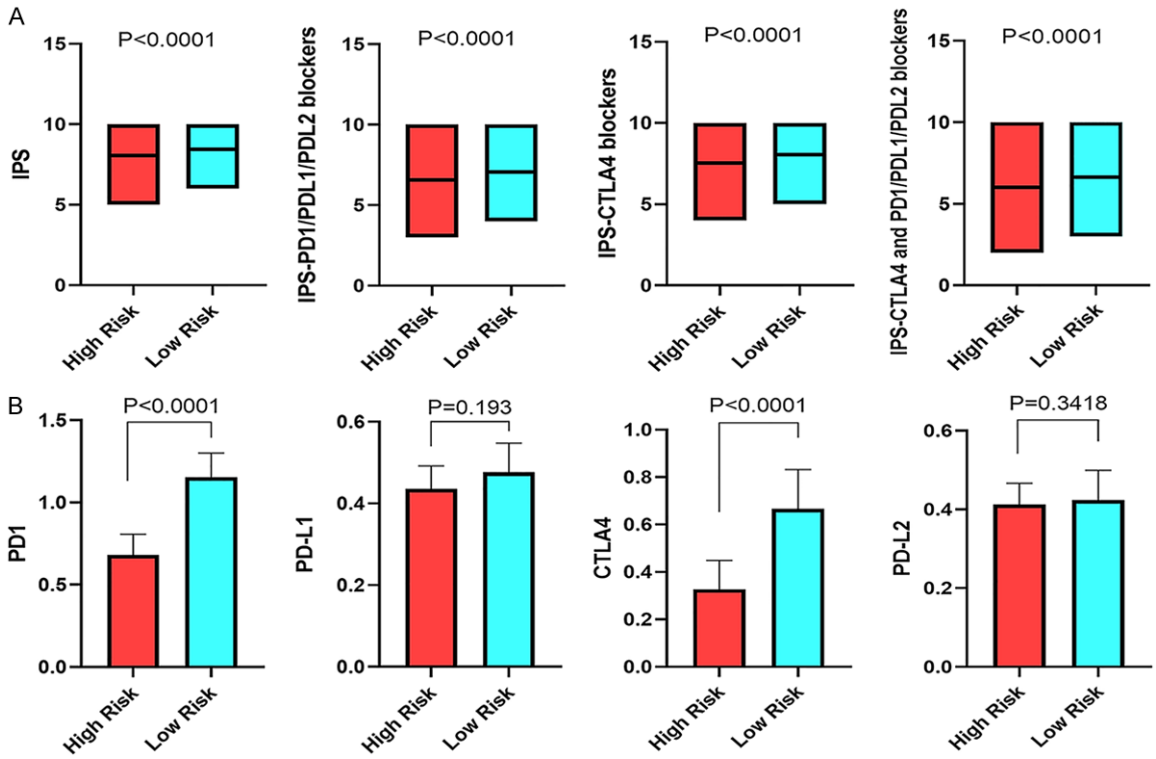

Figure 8. Immunotherapy responses across different risk subgroups. A. Comparison of the IPS between high- and low-risk subgroups. B. Comparison of the expression of ICBs, including PD1, PD-L1, CTLA4, and PD-L2 in high- and low-risk subgroups.

sion [28]. Some cancer cells can acquire an immune escape phenotype by over- or under-expression of certain IRGs, thereby creating a locally immunosuppressed environment [29]. Hence, the expression pattern of IRGs may represent a critical biomarker for patients with EC. Previous studies have demonstrated that ECs with hypermutations of polymerase ε or hypermutated/microsatellite instability were particularly responsive to ICIs [30, 31]. However, other studies indicated that patients with microsatellite stable cancers were insensitive to the anticancer immune response [32]. The complexity of the TME is of great importance, and differences in expression of multiple IRGs may contribute to improve risk assessment in EC, as this approach could screen patients who would benefit from immunotherapy.

Currently, the majority of risk stratification systems applied in EC use the composite of clinical stage (including lymph node involvement and the depth of myometrial invasion), grade, and histologic types [33]. Genomic factors used as predictive biomarkers for EC remains investigational (such as the L1 cell adhesion molecule [L1CAM] and TP53). Besides, the immune risk model has been proven to be more effective than the reliance on a single gene for survival prediction in certain cancers [11, 34]. Based on this premise, we identified an immune-related signature as a biomarker to assess EC prognosis using the TCGA database. The developed signature comprises seven risk IRGs, including four high-risk factors (CBLC, TNF, PLA2G2A, and NR3C1) and three protective factors (APOD, TNFRSF18, and LTB). Among these risk IRGs, four genes (CBLC, TNF, LTB, and TNFRSF18) were overexpressed, while three genes (PLA2G2A, NR3C1, and APOD) showed lower expression in EC samples compared with normal endometrial samples. TNF and TNFRSF18 have been reported to be involved in the onset and progression of EC. A recent study has shown that TNF modulates the course of EC, and high TNF-alpha was associated with poorer disease-specific survival ($P = 0.034$) and recurrence-free survival ($P = 0.049$) [35]. Wang et al. suggested that TNFRSF18 played a protective role in the prognosis of EC, which was consistent with our results [36]. PLA2G2A is also regarded as a potent mediator

of the inflammatory process. Previous studies have demonstrated that higher expression of PLA2G2A was correlated with ovarian endometriosis and deep infiltrating endometriosis [37, 38]. In our study, we found that PLA2G2A may be involved in the pathogenesis of EC and could be used as a biomarker to predict survival. APOD was identified as a protective factor in the current study. Germeyer et al. found that APOD was highly expressed in the endometrium of the proliferative and secretory phases, and participated in the endometrial repair mechanisms [39]. CBLC and LTB genes had been shown to mediate the regulation of the immune response in different cancer and thus, could serve as potential biomarkers for EC [40, 41]. Functional enrichment analysis suggested that DEIRGs were widely involved in the inflammatory process and immune regulation. Cytokine activity may promote the formation of tumor metastasis by modulating the TME [42]. The intracellular MAPK signaling cascade participates in the immune escape response and in cell apoptosis, which promote carcinogenesis [43]. The immune signature we identified exhibited a strong predictive ability in the training, testing, and total cohorts. Furthermore, when combined with clinical variables, our model still remained an independent variable for predicting prognosis of EC.

Tumor-infiltrating immune cells play an important role in modulating the TME status of EC [44]. Kübler et al. reported that the presence of tumor-associated macrophages in EC indicates poor prognosis and aggressive tumor behavior, including advanced-stage, tumor grade, lymphovascular space invasion, and lymph node metastasis [45]. Hu et al. suggested that the infiltration of Tregs and CD8+ T cells in EC samples were associated with a higher rate of MUC16 mutations, which presented a better prognosis [46]. In the present study, we found that the risk score was negatively correlated with the levels of specific immune cells, including T cells CD8, Tregs, NK cells activated, and Dendritic cells resting, which were significantly associated with better prognosis. This result may provide a deeper insight into the immunity of EC.

We evaluated the expression patterns of our immune signature and IPS. The results showed significantly higher scores of IPS, IPS-PD1/PD-L1/PDL2 + CTLA4, IPS-CTLA4, and IPS-PD1/PD-L1/PD-L2 in the low-risk subgroup. Moreover, a higher expression of PD1 and CTLA-4 were also observed in the low-risk subgroup, indicating that our immune signature could help identify patients who would benefit from ICI-based immunotherapy. In addition, a mutational analysis of EC was also performed to explore the signature's prognostic ability. Previous studies have demonstrated that certain gene mutations, such as in PTEN, P53, and POLE, correlated with a favorable prognosis in EC patients [47-49]. Further, a higher hypermutated status might enhance antitumor immune responses [46]. In our study, we found that the TMB was higher in the low-risk subgroup than in the high-risk subgroup, although there was no survival difference between the two groups. These results might further support the classification validity of our immune signature. However, the relationships and underlying mechanisms of the TMB, IPS, and the signature are not yet understood, and further research is needed.

We established a valid immune signature based on seven risk IRGs for survival prediction of EC and its response to immunotherapy. To the best of our knowledge, this is the first study to comprehensively analyze the relationships between EC and the TME and TMB. Besides, we evaluated the correlation between the risk signature and the IPS of EC, which may facilitate clinicians in making individualized treatment choices for targeted therapy. Of note, there were several limitations in the TCGA-based risk model. First, our study was primarily performed using a retrospective database; thus, it requires further validation in in vivo or in vitro trials with larger samples. Second, the available clinical information underreported the comorbidities of the patients, which could significantly impact on EC survival as competing events [50]. Besides, our immune signature only analyzed gene expression values without evaluating the intra-tumor heterogeneity or sampling bias inevitably generated in the process. To resolve the issues mentioned above, we will establish an inhouse EC sample database and incorporate these factors in future model development.

Conclusions

In summary, we constructed and validated a prognostic immune signature for predicting the survival of EC patients. Moreover, our immune

signature may contribute to further stratify patients who are likely to benefit from immunotherapy and will facilitate the application of personalized treatment in the future. To further validate the predictive capability of this model, multicenter testing in clinical trials is needed.

Acknowledgements

We acknowledge the work of Dr. Liu Li involved in the preparation of human endometrial cancer samples and the quantitative real-time PCR (qRT-PCR) analysis.

Disclosure of conflict of interest

None.

Abbreviations

AUC, area under the receiver operating characteristic curve; CTLA4, cytotoxic T lymphocyte antigen 4; Ct, cycle threshold; CI, confidence interval; DEGs, differentially expressed genes; DEIRGs, differentially expressed immune-related genes; DETFs, differentially expressed transcription factors; EC, endometrial cancer; FDR, false-discovery rate; FC, fold change; GO, Gene Ontology; HPA, Human Protein Atlas; HR, hazard ratio; IRGs, immune-related genes; ICIs, immune checkpoints inhibitors; ICBs, Immune checkpoints blockades; IPS, immunophenoscore; KEGG, Kyoto Encyclopedia of Genes and Genomes; OS, overall survival; PD1, programmed cell death 1; PD-L1, programmed cell death-ligand 1; qRT-PCR, quantitative real-time PCR; ROC, receiver operating characteristic; TCGA, The Cancer Genome Atlas; TME, tumor microenvironment; TMB, tumor mutational burden; TFs, transcription factors; TCIA, the Cancer Immunome Atlas; Tregs, T cells regulatory.

Address correspondence to: Dr. Xiaomao Li, Department of Gynecology, The Third Affiliated Hospital of Sun Yat-sen University, No. 600 Tianhe Road, Tianhe District, Guangzhou, Guangdong, China. ORCID ID: https://orcid.org/0000-0001-6374-1488; Tel: +86-13602836078; E-mail: lixmao@mail.sysu.edu.cn

References

[1] Siegel RL, Miller KD and Jemal A. Cancer statistics, 2019. CA Cancer J Clin 2019; 69: 7-34.

[2] Brooks RA, Fleming GF, Lastra RR, Lee NK, Moroney JW, Son CH, Tatebe K and Veneris JL. Current recommendations and recent progress in endometrial cancer. CA Cancer J Clin 2019; 69: 258-279.

[3] Randall ME, Filiaci V, McMeekin DS, von Gruenigen V, Huang H, Yashar CM, Mannel RS, Kim JW, Salani R, DiSilvestro PA, Burke JJ, Rutherford T, Spirtos NM, Terada K, Anderson PR, Brewster WR, Small W, Aghajanian CA and Miller DS. Phase III trial: adjuvant pelvic radiation therapy versus vaginal brachytherapy plus paclitaxel/carboplatin in high-intermediate and high-risk early stage endometrial cancer. J Clin Oncol 2019; 37: 1810-1818.

[4] Zhang L, Kwan SY, Wong KK, Solaman PT, Lu KH and Mok SC. Pathogenesis and clinical management of uterine serous carcinoma. Cancers (Basel) 2020; 76: 37-51.

[5] Sahoo SS, Zhang XD, Hondermarck H and Tanwar PS. The emerging role of the microenvironment in endometrial cancer. Cancers (Basel) 2018; 10: 408-422.

[6] Howitt BE, Shukla SA, Sholl LM, Ritterhouse LL, Watkins JC, Rodig S, Stover E, Strickland KC, D'Andrea AD, Wu CJ, Matulonis UA and Konstantinopoulos PA. Association of polymerase e-mutated and microsatellite-instable endometrial cancers with neoantigen load, number of tumor-infiltrating lymphocytes, and expression of PD-1 and PD-L1. JAMA Oncol 2015; 1: 1319-1323.

[7] Frenel JS, Le Tourneau C, O'Neil B, Ott PA, Piha-Paul SA, Gomez-Roca C, van Brummelen EMJ, Rugo HS, Thomas S, Saraf S, Rangwala R and Varga A. Safety and efficacy of pembrolizumab in advanced, programmed death ligand 1-positive cervical cancer: results from the phase Ib KEYNOTE-028 trial. J Clin Oncol 2017; 35: 4035-4041.

[8] Ott PA, Bang YJ, Berton-Rigaud D, Elez E, Pishvaian MJ, Rugo HS, Puzanov I, Mehnert JM, Aung KL, Lopez J, Carrigan M, Saraf S, Chen M and Soria JC. Safety and antitumor activity of pembrolizumab in advanced programmed death ligand 1-positive endometrial cancer: results from the KEYNOTE-028 study. J Clin Oncol 2017; 35: 2535-2541.

[9] Rubinstein MM and Makker V. Optimizing immunotherapy for gynecologic cancers. Curr Opin Obstet Gynecol 2020; 32: 1-8.

[10] Sfakianaki M, Papadaki C, Tzardi M, Trypaki M, Manolakou S, Messaritakis I, Saridaki Z, Athanasakis E, Mavroudis D, Tsiaoussis J, Gouvas N and Souglakos J. PKM2 expression as biomarker for resistance to oxaliplatin-based chemotherapy in colorectal cancer. Cancers (Basel) 2020; 12: 2058-2072.

[11] Wang Z, Song Q, Yang Z, Chen J, Shang J and Ju W. Construction of immune-related risk sig-

nature for renal papillary cell carcinoma. Cancer Med 2019; 8: 289-304.
[12] Yang S, Wu Y, Deng Y, Zhou L, Yang P, Zheng Y, Zhang D, Zhai Z, Li N, Hao Q, Song D, Kang H and Dai Z. Identification of a prognostic immune signature for cervical cancer to predict survival and response to immune checkpoint inhibitors. Oncoimmunology 2019; 8: e1659094.
[13] Shen S, Wang G, Zhang R, Zhao Y, Yu H, Wei Y and Chen F. Development and validation of an immune gene-set based Prognostic signature in ovarian cancer. EBioMedicine 2019; 40: 318-326.
[14] Guo D, Wang M, Shen Z and Zhu J. A new immune signature for survival prediction and immune checkpoint molecules in lung adenocarcinoma. J Transl Med 2020; 18: 123-137.
[15] Bhattacharya S, Andorf S, Gomes L, Dunn P, Schaefer H, Pontius J, Berger P, Desborough V, Smith T, Campbell J, Thomson E, Monteiro R, Guimaraes P, Walters B, Wiser J and Butte AJ. ImmPort: disseminating data to the public for the future of immunology. Immunol Res 2014; 58: 234-239.
[16] Mei S, Meyer CA, Zheng R, Qin Q, Wu Q, Jiang P, Li B, Shi X, Wang B, Fan J, Shih C, Brown M, Zang C and Liu XS. Cistrome cancer: a web resource for integrative gene regulation modeling in cancer. Cancer Res 2017; 77: e19-e22.
[17] Ritchie ME, Phipson B, Wu D, Hu Y, Law CW, Shi W and Smyth GK. limma powers differential expression analyses for RNA-sequencing and microarray studies. Nucleic Acids Res 2015; 43: e47-e60.
[18] Yu G, Wang LG, Han Y and He QY. clusterProfiler: an R package for comparing biological themes among gene clusters. OMICS 2012; 16: 284-287.
[19] Swartz MD, Yu RK and Shete S. Finding factors influencing risk: comparing Bayesian stochastic search and standard variable selection methods applied to logistic regression models of cases and controls. Stat Med 2008; 27: 6158-6174.
[20] Lorent M, Giral M and Foucher Y. Net time-dependent ROC curves: a solution for evaluating the accuracy of a marker to predict disease-related mortality. Stat Med 2014; 33: 2379-2389.
[21] Zeng F, Liu H, Lu D, Liu Q, Chen H and Zheng F. Integrated analysis of gene expression profiles identifies transcription factors potentially involved in psoriasis pathogenesis. J Cell Biochem 2019; 120: 12582-12594.
[22] Chen B, Khodadoust MS, Liu CL, Newman AM and Alizadeh AA. Profiling tumor infiltrating immune cells with CIBERSORT. Methods Mol Biol 2018; 1711: 243-259.
[23] Mayakonda A, Lin DC, Assenov Y, Plass C and Koeffler HP. Maftools: efficient and comprehensive analysis of somatic variants in cancer. Genome Res 2018; 28: 1747-1756.
[24] Robinson DR, Wu YM, Lonigro RJ, Vats P, Cobain E, Everett J, Cao X, Rabban E, Kumar-Sinha C, Raymond V, Schuetze S, Alva A, Siddiqui J, Chugh R, Worden F, Zalupski MM, Innis J, Mody RJ, Tomlins SA, Lucas D, Baker LH, Ramnath N, Schott AF, Hayes DF, Vijai J, Offit K, Stoffel EM, Roberts JS, Smith DC, Kunju LP, Talpaz M, Cieslik M and Chinnaiyan AM. Integrative clinical genomics of metastatic cancer. Nature 2017; 548: 297-303.
[25] Zaravinos A, Roufas C, Nagara M, de Lucas Moreno B, Oblovatskaya M, Efstathiades C, Dimopoulos C and Ayiomamitis GD. Cytolytic activity correlates with the mutational burden and deregulated expression of immune checkpoints in colorectal cancer. J Exp Clin Cancer Res 2019; 38: 364-382.
[26] Charoentong P, Finotello F, Angelova M, Mayer C, Efremova M, Rieder D, Hackl H and Trajanoski Z. Pan-cancer immunogenomic analyses reveal genotype-immunophenotype relationships and predictors of response to checkpoint blockade. Cell Rep 2017; 18: 248-262.
[27] Lyu X, Jiang Y, Zhang M, Li G, Li G and Qiao Q. Genomic stratification based on radiosensitivity and PD-L1 for tailoring therapeutic strategies in cervical cancer. Epigenomics 2019; 11: 1075-1088.
[28] Quail DF and Joyce JA. Microenvironmental regulation of tumor progression and metastasis. Nat Med 2013; 19: 1423-1437.
[29] Schreiber RD, Old LJ and Smyth MJ. Cancer immunoediting: integrating immunity's roles in cancer suppression and promotion. Science 2011; 331: 1565-1570.
[30] Makker V, Taylor MH, Aghajanian C, Oaknin A, Mier J, Cohn AL, Romeo M, Bratos R, Brose MS, DiSimone C, Messing M, Stepan DE, Dutcus CE, Wu J, Schmidt EV, Orlowski R, Sachdev P, Shumaker R and Casado Herraez A. Lenvatinib plus pembrolizumab in patients with advanced endometrial cancer. J Clin Oncol 2020; 38: 2981-2992.
[31] Grywalska E, Sobstyl M, Putowski L and Rolinski J. Current possibilities of gynecologic cancer treatment with the use of immune checkpoint inhibitors. Int J Mol Sci 2019; 20: 4075-4092.
[32] Di Tucci C, Capone C, Galati G, Iacobelli V, Schiavi MC, Di Donato V, Muzii L and Panici PB. Immunotherapy in endometrial cancer: new scenarios on the horizon. J Gynecol Oncol 2019; 30: e46-e66.

[33] Dong Y, Cheng Y, Tian W, Zhang H, Wang Z, Li X, Shan B, Ren Y, Wei L, Wang H and Wang J. An externally validated nomogram for predicting lymph node metastasis of presumed stage I and II endometrial cancer. Front Oncol 2019; 9: 1218-1229.

[34] Zhao K, Xu L, Li F, Ao J, Jiang G, Shi R, Chen F and Luo Q. Identification of hepatocellular carcinoma prognostic markers based on 10-immune gene signature. Biosci Rep 2020; 40: 1-15.

[35] Wieser V, Abdel Azim S, Sprung S, Knoll K, Kogl J, Hackl H, Marth C, Zeimet AG and Fiegl H. TNFalpha signalling predicts poor prognosis of patients with endometrial cancer. Carcinogenesis 2020; 41: 1065-1073.

[36] Wang Y, Ren F, Chen P, Liu S, Song Z and Ma X. Identification of a six-gene signature with prognostic value for patients with endometrial carcinoma. Cancer Med 2018; 7: 5632-5642.

[37] Sinreih M, Anko M, Kene NH, Kocbek V and Rizner TL. Expression of AKR1B1, AKR1C3 and other genes of prostaglandin F2alpha biosynthesis and action in ovarian endometriosis tissue and in model cell lines. Chem Biol Interact 2015; 234: 320-331.

[38] Carrarelli P, Luddi A, Funghi L, Arcuri F, Batteux F, Dela Cruz C, Tosti C, Reis FM, Chapron C and Petraglia F. Urocortin and corticotrophin-releasing hormone receptor type 2 mRNA are highly expressed in deep infiltrating endometriotic lesions. Reprod Biomed Online 2016; 33: 476-483.

[39] Germeyer A, Capp E, Schlicksupp F, Jauckus J, von Rango U, von Wolff M and Strowitzki T. Cell-type specific expression and regulation of apolipoprotein D and E in human endometrium. Eur J Obstet Gynecol Reprod Biol 2013; 170: 487-491.

[40] Galli G, Proto C, Signorelli D, Imbimbo M, Ferrara R, Prelaj A, De Toma A, Ganzinelli M, Zilembo N, de Braud F, Garassino MC and Lo Russo G. Characterization of patients with metastatic non-small-cell lung cancer obtaining long-term benefit from immunotherapy. Future Oncol 2019; 15: 2743-2757.

[41] Hong SY, Kao YR, Lee TC and Wu CW. Upregulation of E3 ubiquitin ligase CBLC enhances EGFR dysregulation and signaling in lung adenocarcinoma. Cancer Res 2018; 78: 4984-4996.

[42] Shaheen S, Fawaz F, Shah S and Busselberg D. Differential expression and pathway analysis in drug-resistant triple-negative breast cancer cell lines using RNASeq analysis. Int J Mol Sci 2018; 19: 1810-1823.

[43] Kim EK and Choi EJ. Compromised MAPK signaling in human diseases: an update. Arch Toxicol 2015; 89: 867-882.

[44] Iglesia MD, Parker JS, Hoadley KA, Serody JS, Perou CM and Vincent BG. Genomic analysis of immune cell infiltrates across 11 tumor types. J Natl Cancer Inst 2016; 108: 11-22.

[45] Kubler K, Ayub TH, Weber SK, Zivanovic O, Abramian A, Keyver-Paik MD, Mallmann MR, Kaiser C, Serce NB, Kuhn W and Rudlowski C. Prognostic significance of tumor-associated macrophages in endometrial adenocarcinoma. Gynecol Oncol 2014; 135: 176-183.

[46] Hu J and Sun J. MUC16 mutations improve patients' prognosis by enhancing the infiltration and antitumor immunity of cytotoxic T lymphocytes in the endometrial cancer microenvironment. Oncoimmunology 2018; 7: e1487914.

[47] Tao Y and Liang B. PTEN mutation: a potential prognostic factor associated with immune infiltration in endometrial carcinoma. Pathol Res Pract 2020; 216: 152943.

[48] Brett MA, Atenafu EG, Singh N, Ghatage P, Clarke BA, Nelson GS, Bernardini MQ and Kobel M. Equivalent survival of p53 mutated endometrial endometrioid carcinoma grade 3 and endometrial serous carcinoma. Int J Gynecol Pathol 2020.

[49] Li Y, Bian Y, Wang K and Wan XP. POLE mutations improve the prognosis of endometrial cancer via regulating cellular metabolism through AMF/AMFR signal transduction. BMC Med Genet 2019; 20: 202.

[50] van Walraven C and McAlister FA. Competing risk bias was common in Kaplan-Meier risk estimates published in prominent medical journals. J Clin Epidemiol 2016; 69: 170-173, e178.

Table S1. Primer sequences used to amplify target genes by qRT-PCR

Gene name		Primer sequences
CBLC	Forward	5'-GCGCCTAGAAGAGCAATGC-3'
	Reverse	5'-CTCGTCGTTGGCACTCCTT-3'
TNF	Forward	5'-CCTCTCTCTAATCAGCCCTCTG-3'
	Reverse	5'-GAGGACCTGGGAGTAGATGAG-3'
PLA2G2A	Forward	5'-ATGAAGACCCTCCTACTGTTGG-3'
	Reverse	5'-GCTTCCTTTCCTGTCGTCAACT-3'
NR3C1	Forward	5'-ACAGCATCCCTTTCTCAACAG-3'
	Reverse	5'-AGATCCTTGGCACCTATTCCAAT-3'
APOD	Forward	5'-ACAAGCATTTCATCTTGGGAAGT-3'
	Reverse	5'-CATCAGCTCTCAACTCCTGGT-3'
TNFRSF18	Forward	5'-ACCCAGTTCGGGTTTCTCAC-3'
	Reverse	5'-CCAGATGTGCAGTCCAAGC-3'
LTB	Forward	5'-GGAGACGACGAAGGAACAGG-3'
	Reverse	5'-GTAGAGGTAATAGAGGCCGTCC-3'
GAPDH	Forward	5'-AGAAGGCTGGGGCTCATTTG-3'
	Reverse	5'-AGGGGCCATCCACAGTCTTC-3'

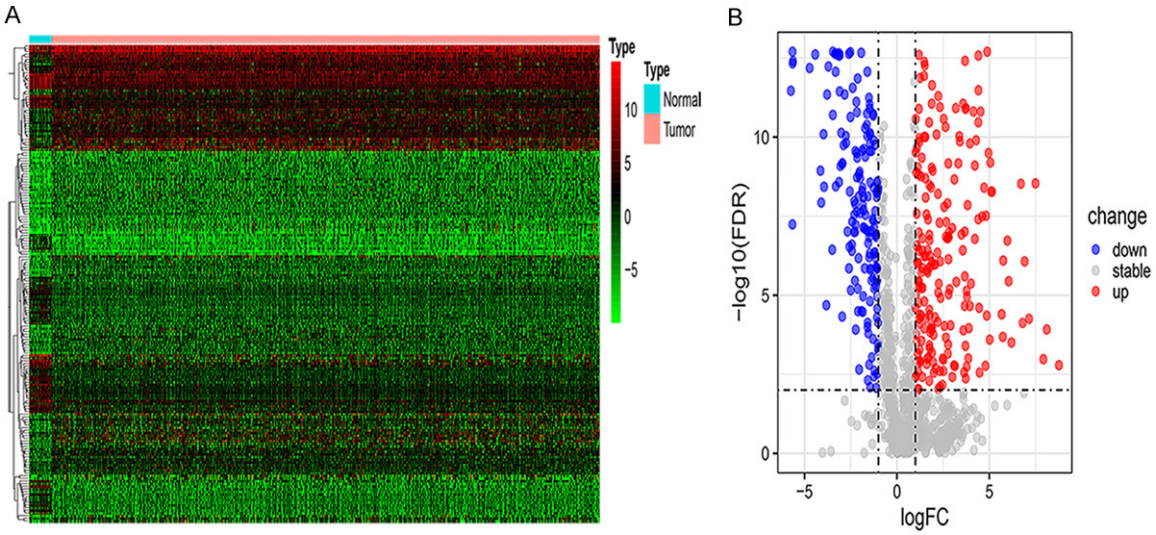

Figure S1. Identification of DEIRGs between EC samples and adjacent normal samples. A. Heatmap of DEIRGs; the red to green spectrum indicates high to low genes expression. B. Volcano plot of DEIRGs.

Table S2. Identification of OS-related DEIRGs in univariate analysis

Id	HR	HR.95 Low	HR.95 High	*P*-value
COLEC12	1.034147508	1.003354928	1.065885102	0.029470835
IL6	1.016114383	1.003934243	1.028442298	0.009373422
APOD	0.980081662	0.961078152	0.999460932	0.04401594
TNF	1.033384881	1.012874147	1.054310958	0.001324717
PLA2G2A	1.032546638	1.006483498	1.05928469	0.014072387
PDGFRA	1.026468498	1.00190481	1.051634412	0.034519285
TNFSF11	0.708988111	0.504824849	0.995719887	0.047175942
RAC3	1.012374161	1.001953011	1.022903699	0.019830215
FGF18	1.007797494	1.001368127	1.014268141	0.017375934
LTB	0.978826205	0.960899671	0.997087177	0.02325153
GHR	2.518167349	1.217213598	5.20957604	0.012777265
NPR1	1.01951431	1.007841382	1.031322435	0.001004106
NR2F1	1.017046616	1.00240859	1.031898398	0.022300925
NR3C1	1.187482462	1.075701624	1.310878934	0.000657608
THRB	1.21546853	1.091688555	1.35328317	0.000369689
TNFRSF18	0.965789461	0.940434247	0.991828282	0.010333669
VIPR2	0.312895564	0.114101788	0.858037684	0.023980762
CBLC	1.011341836	1.00530124	1.017418729	0.000224466

Table S3. The relationship between DEIRGs and DETFs in the network

DETFs	DEIRGs	correlation	*P*-value	Regulation
ATF3	IL6	0.308031404929953	1.62114235550776e-12	positive
ATF3	TNF	0.266285554139827	1.30169007189794e-09	positive
ATF3	THRB	0.216931212632701	9.02603150282224e-07	positive
CBX2	RAC3	0.363774253945774	3.49214962694847e-17	positive
CBX7	GHR	0.279541553691605	1.75336619303748e-10	positive
CBX7	NR3C1	0.377395071059455	1.79622745686738e-18	positive
CBX7	VIPR2	0.231368755245739	1.54162097737631e-07	positive
CENPA	RAC3	0.357439906777772	1.32373713844432e-16	positive
CENPA	FGF18	0.204577508521719	3.73169370147434e-06	positive
CENPA	NPR1	0.226035363058598	3.00256874554863e-07	positive
E2F1	RAC3	0.485199105403187	4.57961528279263e-31	positive
EBF1	GHR	0.256270332369018	5.51300430443539e-09	positive
EBF1	NR3C1	0.224424978336333	3.66038205619704e-07	positive
EGR1	IL6	0.226980671967709	2.67111348761324e-07	positive
EGR1	TNF	0.265434774432312	1.47497736335668e-09	positive
ELF5	PLA2G2A	0.306755737758867	2.02198510605108e-12	positive
EZH2	RAC3	0.293419613227561	1.91114497832589e-11	positive
FOS	IL6	0.232413312101021	1.35035285155692e-07	positive
FOS	TNF	0.274679503397533	3.70405494528926e-10	positive
FOS	PDGFRA	0.216471191683418	9.53041458237046e-07	positive
FOXA2	NPR1	-0.278630150497621	2.01950327083339e-10	negative
FOXA2	NR3C1	-0.251889619746694	1.01710149178932e-08	negative
FOXA2	THRB	-0.32299917844869	1.11879059832644e-13	negative
FOXM1	RAC3	0.308065737943435	1.6115068328927e-12	positive
FOXP3	TNFSF11	0.270735467001749	6.72179718026405e-10	positive
FOXP3	NR3C1	0.264780705357728	1.6232423865395e-09	positive

FOXP3	VIPR2	0.216675693742079	9.30293825384315e-07	positive
GATA6	NR3C1	0.246097826886221	2.24605446643314e-08	positive
H2AFX	RAC3	0.318573325254082	2.50539268516018e-13	positive
LHX2	RAC3	0.240012508028483	5.05456206027217e-08	positive
LMNB1	RAC3	0.226617600701285	2.79402194460599e-07	positive
MAF	GHR	0.334651832317134	1.25620784176445e-14	positive
MAF	NR2F1	0.323097297925051	1.09880640276601e-13	positive
MAF	NR3C1	0.304777438458751	2.84228323906343e-12	positive
MAF	VIPR2	0.214158413214049	1.25042593045682e-06	positive
MITF	RAC3	-0.20201238324329	4.95799474079648e-06	negative
MITF	NR3C1	0.293909300493047	1.76342808708356e-11	positive
MITF	VIPR2	0.239503298778673	5.40423883788499e-08	positive
MYBL2	RAC3	0.276601034385597	2.76104676579287e-10	positive
MYH11	GHR	0.327008637256549	5.32797665558483e-14	positive
MYH11	NR3C1	0.228774926398931	2.13629545646838e-07	positive
NCAPG	RAC3	0.261618395380238	2.56987644518618e-09	positive
NR2F1	GHR	0.227670583814222	2.45175545096717e-07	positive
NR2F2	NR2F1	0.263567251956419	1.93757539706772e-09	positive
NR2F2	NR3C1	0.225422868647448	3.2381007692353e-07	positive
NR2F2	VIPR2	0.488978626862818	1.35629695067881e-31	positive
NR3C1	GHR	0.310564292966182	1.04210390047694e-12	positive
NR3C1	NPR1	0.266340210338777	1.29126122186693e-09	positive
NR3C1	THRB	0.302509985591805	4.1860258706315e-12	positive
NR4A1	IL6	0.27042857740235	7.03799742105166e-10	positive
NR4A1	TNF	0.256578921803519	5.27794182670655e-09	positive
PBX1	GHR	0.343381320651369	2.29447231842922e-15	positive
PBX1	NR3C1	0.219004838881719	7.05355856454856e-07	positive
PBX3	GHR	0.211179093667132	1.76638883258687e-06	positive
PBX3	NR2F1	0.251150653670508	1.12652729945585e-08	positive
PBX3	NR3C1	0.301015524051666	5.39287963846918e-12	positive
SNAI2	PDGFRA	0.410515190801987	7.1917765099664e-22	positive
SNAI2	GHR	0.383715663552757	4.31857872949359e-19	positive
SOX17	NR3C1	-0.241844526202412	3.9684610861226e-08	negative
SPDEF	NPR1	-0.262059863844956	2.41110067549646e-09	negative
SPDEF	NR3C1	-0.245800205614768	2.33812648774133e-08	negative
SPDEF	THRB	-0.280276570372464	1.56391848042475e-10	negative

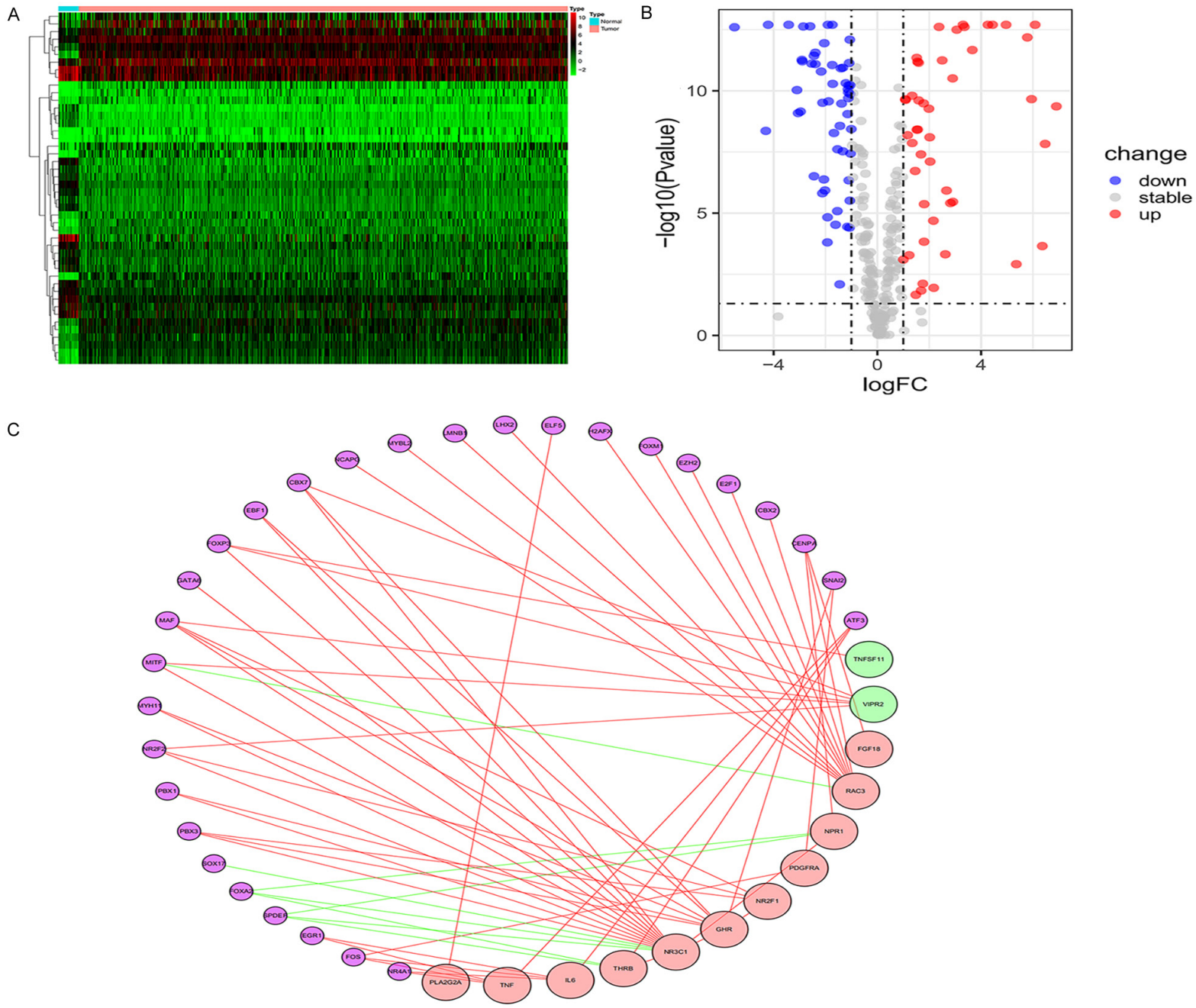
A
Type
Normal
Tumor
B
−log10(Pvalue)
logFC
change
down
stable
up
C
LHX2
ELF5
H2AFX
FOXM1
EZH2
E2F1
CBX2
CENPA
SNAI2
ATF3
TNFSF11
VIPR2
FGF18
RAC3
NPR1
PDGFRA
NR2F1
GHR
NR3C1
THRB
IL6
TNF
PLA2G2A
NR4A3
FOS
EGR1
SPDEF
FOXA2
SOX17
PBX3
PBX1
NR2F2
MYH11
MITF
MAF
GATA2
FOXP3
EBF1
CBX7
KCAP0
HYBL2
MNB1

Figure S2. The prognostic DEIRGs-DETFs regulatory networks. A. Heatmap of DETFs; the red to green spectrum indicates high to low TF expression. B. Volcano plots of DETFs. C. Regulatory network of the prognostic DEIRGs and DETFs; the red circles indicate prognostic DEIRGs with hazard ratios > 1 (P < 0.05), the green circles indicate prognostic DEIRGs with hazard ratios < 1 (P < 0.05); the purple circles indicate DETFs involved in regulation of gene expression (correlation coefficient > 0.3, P < 0.05), the green lines represent negative regulatory relationships, and the red lines represent positive regulatory relationships.

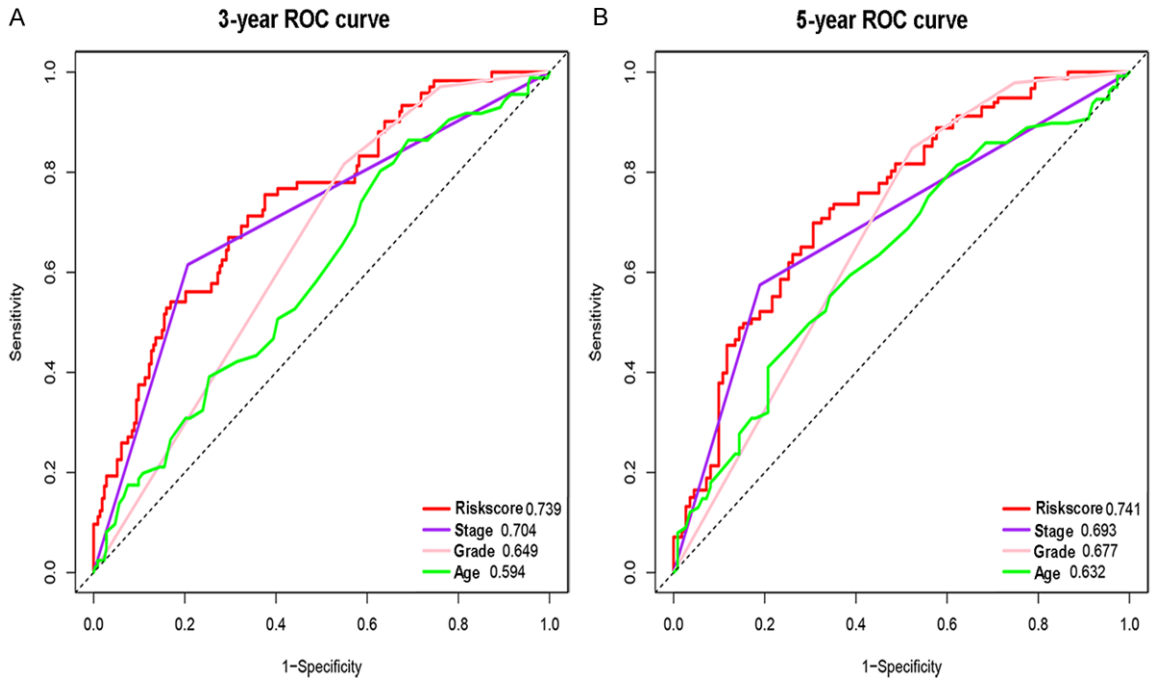

Figure S3. Time-dependent ROC curves of immune signature and clinical factors in the total TCGA cohort at three and five year. A. ROC curves at 3-years. B. ROC curves at 5-years.

Table S4. The correlation analysis between the immune signature and clinical variables

Immune signature	Age t-test (*P*)	Grade t-test (*P*)	Stage t-test (*P*)	Histological type t-test (*P*)
APOD	2.075 (0.039)	52.821 (3.389E-12)	3.538 (4.428E-04)	9.72 (0.008)
TNF	-2.244 (0.025)	1.858 (0.395)	-1.811 (0.072)	15.994 (3.364E-04)
PLA2G2A	-0.084 (0.933)	12.763 (0.002)	-1.053 (0.294)	2.617 (0.270)
LTB	-1.332 (0.184)	-7.231 (0.027)	-0.475 (0.635)	4.257 (0.119)
NR3C1	-1.992 (0.047)	28.477 (6.551E-07)	-2.805 (0.005)	57.893 (2.683E-13)
CBLC	-1.424 (0.156)	0.175 (0.916)	-0.93 (0.354)	5.8 (0.055)
TNFRSF18	0.363 (0.717)	9.998 (0.007)	1.75 (0.081)	13.555 (0.001)
Risk score	-1.482 (0.140)	62.061 (3.339E-14)	-1.778 (0.078)	47.751 (4.276E-11)